Insect Biochemistry and Molecular Biology 111 (2019) 103175

Contents lists available at ScienceDirect

Insect Biochemistry and Molecular Biology

journal homepage: www.elsevier.com/locate/ibmb

Developmental and transcriptomic features characterize defects of silk gland growth and silk production in silkworm naked pupa mutant

Wenbo Hu[a,b], Yulin Chen[a,b], Ying Lin[a,b], Qingyou Xia[a,b,*]

[a] Biological Science Research Center, Southwest University, Chongqing, 400716, PR China
[b] Chongqing Key Laboratory of Sericulture Science, Chongqing Engineering and Technology Research Center for Novel Silk Materials, Beibei, Chongqing, 400716, PR China

ARTICLE INFO

Keywords:
Silkworm
Silk gland degeneration
Fibroin secretion-deficiency
Cellular stress responses
Naked pupa mutant
Transcriptome

ABSTRACT

The silkworm *Bombyx mori* is a well-characterized model organism for studying the silk gland development and silk production process. Using positional cloning and gene sequencing, we have previously reported that a truncated fibroin heavy chain was responsible for silkworm naked pupa (*Nd*) mutant. However, the mechanisms by which the mutant FibH causes developmental defects and secretion-deficiency of the silk gland remain to be fully elucidated. Here, silk gland's developmental features, histomorphology, and transcriptome analyses were used to characterize changes in its structure and gene expression patterns between *Nd* mutant and WT/Dazao. Whole larval stage investigation showed that *Nd*-PSG undergoes an arrested/delayed development, which eventually resulted in a gland degeneration. By using section staining and transmission electron microscope, a blockade in intracellular vesicle transport from endoplasmic reticulum to Golgi apparatus (secretion-deficiency) and an increased number of autophagosomes and lysosomes were found in *Nd*-PSG's cytoplasm. Next, by using RNA sequencing and comparative transcriptomic analysis, 2178 differentially expressed genes were identified between *Nd*-PSG and WT-PSG, among which most of the DEGs associated with cellular stress responses (autophagy, ubiquitin-proteasome system, and heat shock response) were significantly up-regulated in *Nd*-PSG, suggesting that mutant FibH perturbed cellular homeostasis and resulted in an activation of adaptive responses in PSG cells. These findings reveal the molecular mechanism of the *Naked pupa* (*Nd*) mutation and provide insights into silk gland development as well as silk protein production in silkworm *Bombyx mori*.

1. Introduction

Silks are externally spun fibrous, proteinaceous materials with biological activities, and have excellent mechanical properties (Omenetto and Kaplan, 2010; Vepari and Kaplan, 2007). Many distantly related insect species from orders Lepidoptera, Trichoptera, Embioptera, Hymenoptera, Coleoptera, Thysanura, Neuroptera, and Prosoptera use silk for various purposes (Craig, 1997; Liu and Zhang, 2014). The domesticated silkworm *Bombyx mori*, a lepidopteran insect with important economic value, produces large amounts of silk for cocoons used during the metamorphosis from larvae to moths. Silk gland is the only organ for producing, storing, and processing silk fibers, and its development, as well as the synthesis of the silk protein, are two of the most important issues in silkworm studies (Xia et al., 2014). Understanding the molecular mechanisms of the development of the silk glands and the process of silk protein production is crucial for increasing silk yield through improvements in the rearing conditions, through breeding, or through genetic manipulation (Ma et al., 2011, 2014).

The silk glands in *Bombyx mori* originate from labial salivary glands, which explains why the silk fiber exits through a pore on the lower lip of the mouth of the silkworm (Andersson et al., 2016; Sutherland et al., 2010). The silk glands are paired and can be divided into three morphologically distinct regions: the posterior silk gland (PSG), the middle silk gland (MSG), and the anterior silk gland (ASG) (Asakura et al., 2007). Silk fibroins, a 2300 kDa molecular complex, consisting of six sets of disulfide-linked fibroin heavy (FibH, 350 kDa) and light (FibL, 25 kDa) chains and a fibrohexamerin protein (P25, 30 kDa) at a molar ratio of 6:6:1 (Aramwit et al., 2012; Inoue et al., 2000), is synthesized in the PSG. Silk sericin, an adhesive protein that accounts for 25–30% of

Abbreviations: Nd, naked pupa; L5D3, the 3rd day of the fifth larval instar; ASG, anterior silk gland; MSG, middle silk gland; PSG, posterior silk gland; FPKM, fragments per kilobase of transcript sequence per millions base pairs sequenced; KEGG, Kyoto Encyclopedia of Genes and Genomes; FibH, fibroin heavy chain; FibL, fibroin light chain; CT, C terminal domain; ER, endoplasmic reticula; Go, the Golgi apparatus

* Corresponding author. Biological Science Research Center, Southwest University, Chongqing, 400716, China.
E-mail address: xiaqy@swu.edu.cn (Q. Xia).

https://doi.org/10.1016/j.ibmb.2019.05.010
Received 11 April 2019; Received in revised form 23 May 2019; Accepted 26 May 2019
Available online 28 May 2019
0965-1748/

the total *B. mori* cocoon by weight (Xia et al., 2014), is synthesized in the MSG. The ASG forms a duct through which silk flows to form a solid silk fiber in the spinneret (Wang et al., 2015).

Silk gland morphogenesis is completed in the embryo 24–48 h before hatching. This process appears to be regulated by homeobox genes, such as *Antennapedia* (*Antp*), *even-skipped* (*eve*), *Sex combs reduced* (*Scr*), *Ultrabithorax* (*Ubx*), *Deformed*, and *Pax6* (Dhawan and Gopinathan, 2003; Kokubo et al., 1997). The number of cells in the glands increases only during the embryonic stage, and each silk gland (ASG, MSG, and PSG) is eventually composed of approximately 1000 cells (300, 250, and 450 cells, respectively) (Kokubo et al., 1996, 1997; Sehnal and Akai, 1990). Following differentiation, the silk gland cells stop dividing but undergo endomitosis (chromosomal endoreduplication) without an increase in the cell number during each of the five larval instars (Xia et al., 2014), which accompanied by gland cell renewal during the molt to intermolt transition process (Hu et al., 2016). As a result, the volume of the cells increases dramatically and rapidly. Multiple rounds of DNA replication result in a 200,000- to 400,000-fold increase in DNA content at the end of the larval stage (Perdrix-Gillot, 1979).

Silkworm fibroin-deficient (naked pupa) mutants, *Nd*, *Nd-s*, and *Nd-s^{D}*, are characterized by developmental abnormalities (degeneration) in PSG, reduced silk fibroin production, and poor cocooning (Mori et al., 1995; Nakano, 1951; Takei et al., 1987), which serve as useful resources for studying multiple aspects of silk gland development and silk formation (Goldsmith et al., 2005). Molecular genetic studies have revealed the importance of the disulfide bonds between FibH and FibL for the efficient secretion of fibroin from the PSG cells to lumen using the *Nd-s* and *Nd-s^{D}* mutants (exons replacement in *FibL*) (Mori et al., 1995; Takei et al., 1987). In our previous study, the molecular basis of the *Nd* mutant known since 1933 was explored: a deletion of 19 bp in A07 of *FibH* leads to premature translational termination and results in a truncated FibH (Hu et al., 2019). Although the genomic defects of these naked silkworms have been clearly explored, the variation of the detailed molecular mechanism of silk gland development and silk proteins synthesized in these mutants is still poorly known, according to published reports.

In this study, we targeted the dominated naked silkworm (*Nd* mutant) characterized by abnormal development of the PSG and reduced silk production. The comprehensive analyses of the silk gland developmental and transcriptomic features were performed between *Nd* mutant and wild-type strain Dazao (WT/Dazao). The silk gland growth during the larval stages between the first and fifth instars and its subcellular structure in fibroin secretion process were observed. The differentially expressed genes between degenerated PSG of *Nd* mutant and normal developed PSG of WT/Dazao were analyzed and a batch of genes involved in cellular stress responses were identified. These results explored the molecular mechanism of silk gland degeneration and fibroin secretion-deficiency in silkworm *Nd* mutant, which might provide novel insight into the understanding of silk gland development and silk secretion process during the larval stage.

2. Materials and methods

2.1. Silkworm strains

Mutant strains for *Naked pupa* (*Nd*), and wild-type strain Dazao (WT/Dazao) were obtained from the Silk Science and Technology Research Group, Southwest University (Chongqing, China). Silkworms were reared on fresh mulberry leaves at a constant temperature of 25 °C on a 12: 12 h light: dark cycle.

2.2. Larval silk gland morphological observations

Silk glands at each larval instar in the life cycle were dissected in phosphate buffered saline (PBS, pH 7.4) and fixed three times for 10 min each in methanol. Nucleus staining was conducted for 10 min using DAPI. Fluorescence images for observations of nuclei were captured using a BX51 fluorescence microscope (Olympus, Japan). Linear measurements (n = 8) were acquired using an Axio Imager.A2 microscope (Zeiss, Germany) and SZM-45B3 zoom stereo microscope (Sunnyoptical, China).

2.3. Silk gland cell count

Silk glands of neonate larvae were dissected in PBS and fixed three times for 10 min each in methanol. Nucleus staining was conducted for 10 min using DAPI. Fluorescence images were captured using a BX51 fluorescence microscope (Olympus, Japan). The cell number of MSG and PSG were analyzed by counting the number of their nuclei respectively (n = 7).

2.4. Silk gland DNA measurement

Silk glands from L5D7 larval stages were dissected in PBS and divided into MSG and PSG. Total DNA was extracted from silk gland using DNeasy Blood & Tissue Kit (QIAGEN, Germany). The amount of DNA was measured using a Qubit 2.0 Fluorometer (Life Technologies, USA) (n = 3).

2.5. Silk gland isolation and sections

Fresh silk glands from L5D7 larval stages were dissected in PBS and divided into MSG and PSG. Both parts were fixed using 4% (v/v) paraformaldehyde/PBS, dehydrated in a gradient ethanol series from 70% to 100%, embedded in paraffin, and cut into 5-μm sections. After deparaffinizing, silk gland sections were examined by bright-field microscopy Images of the sections were captured using the Axio Imager 2 microscope (Zeiss, Germany).

2.6. Transmission electron microscope (TEM) observations

Fresh silk gland parts were dissected in PBS on ice, cut into 1 mm^3 sections, and fixed in ice-cold 2.5% glutaraldehyde solution (Sigma-Aldrich, USA) for 24 h. Silk gland sections were then dehydrated in an ethanol series from 50% to 90%, embedded in Spurr resin (Spi-Chem, USA), cured, and cut into 70-nm sections. Sections were stained using 3% uranyl acetate-lead citrate (Spi-Chem, USA). Images were captured using a JEM1230 transmission electron microscope (JEOL, Japan).

2.7. RNA preparation, transcriptome sequencing, and mapping

Total RNA of PSG from *Nd* mutants and WT/Dazao were prepared using TRIzol reagent (Invitrogen, USA) as described previously (Hu et al., 2016). RNA quality and quantity were analyzed using an Agilent Bioanalyzer 2100 system (Agilent Technologies, USA) and the Qubit RNA Assay Kit (Life Technologies, USA). Transcript library preparation, clustering, and sequencing of the four RNA samples (two biological replicates per condition) were performed by Beijing Novogene Bioinformatics Technology Co., Ltd. Sequencing libraries were generated using NEBNext Ultra RNA Library Prep Kit for Illumina (NEB, USA) following the manufacturer recommendations, and index codes were added to attribute sequences to each sample. Briefly, mRNAs were enriched using poly-T oligo-attached magnetic beads and fragmented into short pieces in a fragmentation buffer. Then, the first and second strand cDNAs were synthesized using a random hexamer primer. Following selection and purification of the cDNA fragments, sequencing adaptors were ligated to cDNA fragments during PCR amplification. RNA libraries were constructed using Illumina TruSeq RNA preparation kits following the manufacturer instructions. Sequencing of the eight samples was conducted using an Illumina HiSeq 2000 platform (Illumina, USA), and 125–150 bp paired-end reads were generated.

The raw data (raw reads) in fastq format were processed using in-

house Perl scripts. Paired-end clean reads were mapped to the silkworm genome (Wang et al., 2005; Xia et al., 2004) using TopHat v2.0.12 (Trapnell et al., 2012). The number of reads mapped to each gene was counted using HTSeq v0.6.1 (Anders et al., 2015), and the FPKM of each gene was calculated based on gene length and the number of reads mapped to each gene (Trapnell et al., 2010).

2.8. Total RNA extraction and qRT-PCR

Total silk gland (MSG and PSG) RNA was extracted from the *Nd* mutant and WT/Dazao using TRIzol reagent (Invitrogen, USA). Reverse transcription was performed on total RNA (1 mg) using a random primer (N6), an oligo (dT) primer, and the PrimeScript RT reagent Kit using gDNA Eraser (Takara, Japan) according to the manufacturer's protocols. The qRT-PCR was performed using a qTOWER 2.0 real-time PCR system (Analytik Jena, Germany) and SYBR *Premix Ex Taq* II (Takara, Japan) according to the manufacturer's protocols. The silkworm housekeeping gene *ribosomal protein L3* (*Rpl3*: GenBank accession number NM_001043661.1) was used as the internal control for RNA normalization. Primer sets for qRT-PCR are listed in Table S6. Three independent replicates were analyzed.

2.9. Differentially expressed genes (DEGs) and pathways analysis

Differential expression analysis of two conditions was conducted using the DESeq R package v1.18.0 (Anders and Huber, 2010). DESeq provides statistical routines for determining differential expression in digital gene expression data using a model based on the negative binomial distribution. The *P* values were adjusted using the Benjamini & Hochberg method for controlling the false discovery rate. An adjusted *P* value (*P*adj) below 0.005 and a $\log_2$ (fold change in read count) of 1 were set as thresholds for significant differential expression. KOBAS software (Xie et al., 2011) was used to test the statistical enrichment of DEGs in the KEGG pathways (Kanehisa and Goto, 2000), with *P*adj below 0.05 considered to represent significantly enriched DEGs.

2.10. Statistical analysis

Statistical differences were evaluated using Student's *t*-test for unpaired samples. The level of statistically significant difference was set at * P value $<$ 0.05, ** P value $<$ 0.01, and *** P value $<$ 0.001.

3. Results

3.1. Developmental defects of the Nd-PSG during the larval stage

During the development of the silk gland in the larval stage of *B. mori*, the gland cell number remains constant while the gland volume increases (Xia et al., 2014). To characterize developmental features of the silk gland in *Nd* mutant, firstly, we measured the length of the silk gland at each larval instar. The length of *Nd*-MSG and WT-MSG increased at a consistent rate (Fig. 1A); however, the length of *Nd*-PSG increased at a significantly lower rate than in WT-PSG from the 1st day of the fourth instar (L4D1) onwards (Fig. 1B). Secondly, we compared the number of silk gland cells by staining nuclei (Fig. 1C). No significant difference in the number of MSG and PSG cells between *Nd* mutants and WT/Dazao was observed (Fig. 1D), suggesting that the short PSG in *Nd* mutants was not generated by a decrease in cell number. At the end of the larval stage, the length of *Nd*-PSG was less than a quarter that of WT-PSG (Fig. 1B), and the amount of DNA in degenerate *Nd*-PSG was only about a third of that in WT-PSG (Fig. 1E). These results revealed developmental defects in a gland volume increase of *Nd*-PSG during the larval stage.

3.2. Nucleus ramification of the silk gland cells at each larval instar

Nucleus ramification of the silk gland cells develops gradually as the larvae grow, that plays a major role in the increase of silk gland volume, and considerably enlarges the nucleus surface to facilitate the transfer of materials related to the silk synthesis (Akai, 1983). To further characterize cellular developmental defects in a gland volume increase of *Nd*-PSG, we investigated the transformation of the nuclear shape of silk gland cells during larval development. As shown in Fig. 2A and B, for normally developed silk gland parts (*Nd*-MSG, WT-MSG, and WT-PSG), the nuclear ramifications appeared at the L4D1 and developed gradually since then; however, in *Nd*-PSG, the nuclear ramification was reduced/smaller/lesser and delayed to the L5D3 (Fig. 2B). These observations suggested that the *Nd*-PSG undergoes an arrested/delayed development during the larval stage.

3.3. Silk gland histomorphology and section observation

The last larval instar (fifth instar) is the period during which the most vigorous silk protein synthesis and secretion occur in the silk gland (MSG and PSG) of *B. mori*. Anatomical observations of the silk gland at the fifth larval instar showed that no significant difference was exhibited in MSG between *Nd* mutant and WT/Dazao, and the PSG of the WT/Dazao was long and folded, while that of *Nd* mutant was extremely short and degenerate (Fig. 3A). Then, we investigated silk protein (sericin and fibroin) distributions in silk gland lumen. Silk gland section observation showed that WT-PSG was filled with fibroin, and WT-MSG were filled with fibroin and sericin, however, only a small portion of fibroin was secreted into the *Nd*-PSG lumen, which caused a fibroin-absent sericin to be stored in the *Nd*-MSG lumen (Fig. 3B). These findings imply that silk fibroin secretion in degenerated *Nd*-PSG is deficient.

3.4. Intracellular transport and secretion deficiency of fibroin in Nd-PSG

To further investigate the cellular secretion-deficiency resulting from *Nd* mutation (a truncated FibH), we performed ultrastructural observations of *Nd*-PSG (Fig. 4A) using a transmission electron microscope (TEM). As shown in Fig. 4B, the fibroin intracellular transport and secretion process in the cytoplasm of *Nd*-PSG was not observed; this was replaced with an increased number of spotted autophagosomes, which are characterized with double membranes and cellular contents (Franzetti et al., 2012; Xie et al., 2016), and lamellar structures, which are precursors of autophagosomes (Akai, 1979; Morimoto et al., 1968), in the cytoplasm of *Nd*-PSG compared with WT-PSG. In addition, for *Nd*-PSG, the endoplasmic reticulum (ER) were distended, the Golgi apparatus (Go) were poorly developed, and proteins were accumulated in the ER and could not be transported to the Golgi apparatus compared with that in WT-PSG (Fig. 4B and C). Organelles volume analysis showed ten times distended ER and five times reduced Go in *Nd*-PSG compared with WT-PSG (Fig. 4C). These results suggest that the mutant FibH induced a breakdown in the intracellular protein transport system, and the basic fibroin secretion system of *Nd*-PSG was disrupted.

3.5. Comparative transcriptomic analysis and statistics of gene expression

The FibH is a structural protein with no catalytic or regulatory function. To precisely understand the molecular mechanism of silk gland developmental defects and fibroin secretion-deficiency caused by the mutant FibH, we prepared total RNA from PSG at the L5D3 and conducted RNA-seq to identify the differentially expressed genes (DEGs) in *Nd*-PSG and WT-PSG. In total, 118,811,600 raw reads were obtained from the *Nd*-PSG, 107,872,742 from the WT-PSG. The ratios of clean reads, which were obtained by removing low-quality reads, were 97.05% for the *Nd*-PSG and 96.49% for the WT-PSG. Values of Q20 $>$ 93% in all quality scores and GC contents ranging from 45.34%

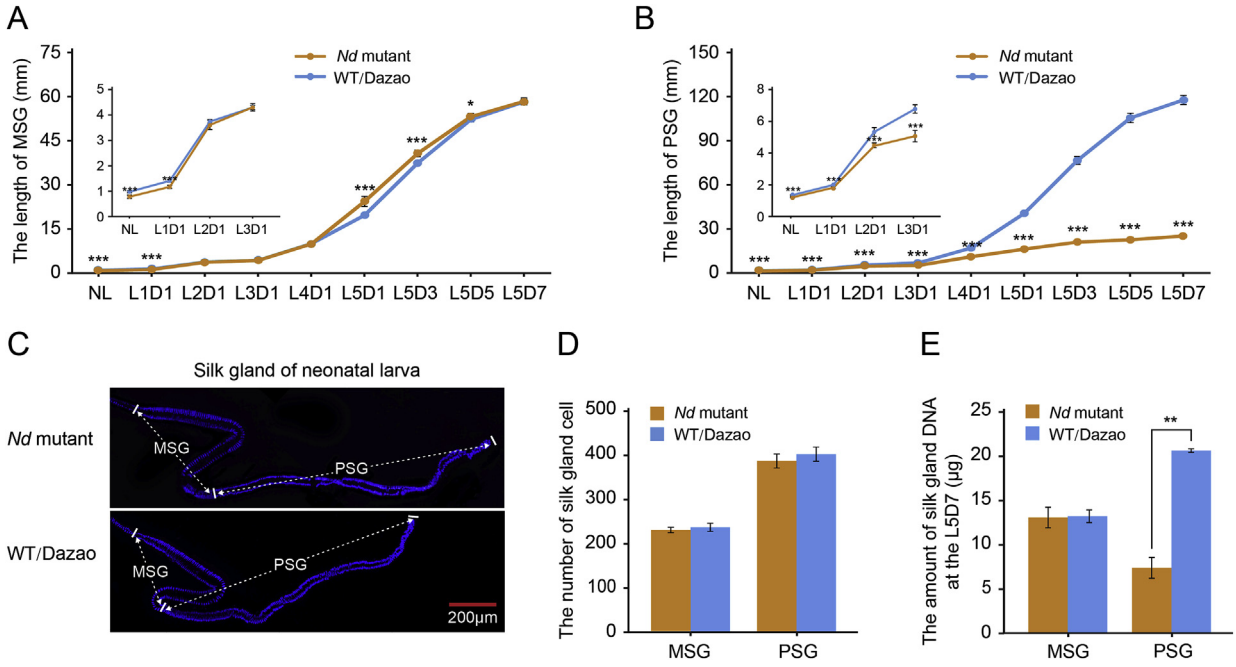

Fig. 1. Developmental defects of the *Nd*-PSG during the larval stage. (A, B) The length of the MSG (A) and PSG (B) at each larval instar. NL indicates the neonatal larval stage, Values are means ± SD (n = 8). (C) Silk gland nucleus staining of the neonatal larva. Cell nuclei are shown in blue. (D) The number of silk gland cells in *Nd* mutants and WT/Dazao. Values are means ± SD (n = 7). (E) The amount of silk gland DNA at the L5D7. Values are means ± SD (n = 3). Asterisks represent significant differences determined by a Student's *t*-test at *P* value < 0.05 (*), 0.01 (**), *P* value < 0.001 (***). (For interpretation of the references to color in this figure legend, the reader is referred to the Web version of this article.)

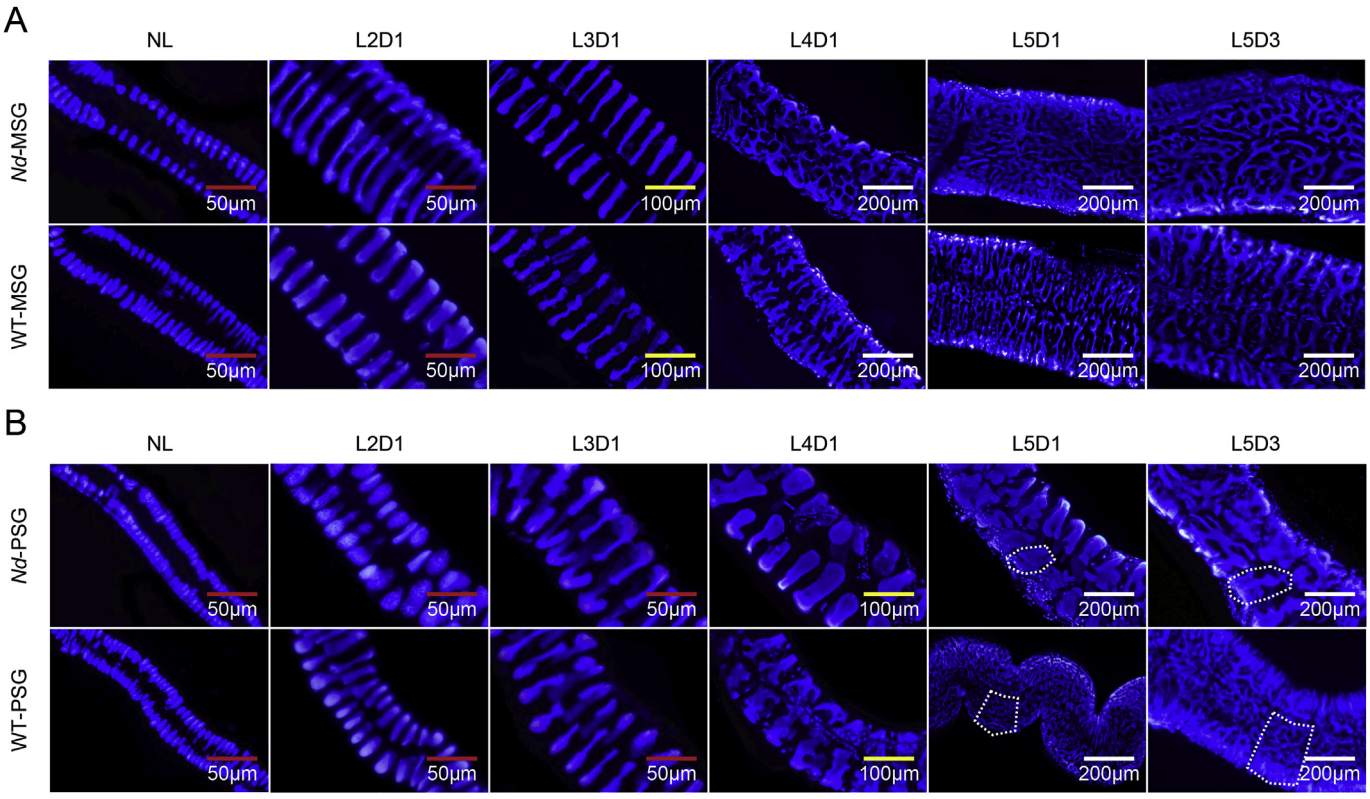

Fig. 2. Nucleus ramification of the silk gland cells at each larval instar. (A) Silk gland nucleus staining of the MSG at each larval instar. (B) Silk gland nucleus staining of the PSG at each larval instar. Cell nuclei are shown in blue. Dotted box indicates the single cell of the PSG. NL indicates the neonatal larval stage. (For interpretation of the references to color in this figure legend, the reader is referred to the Web version of this article.)

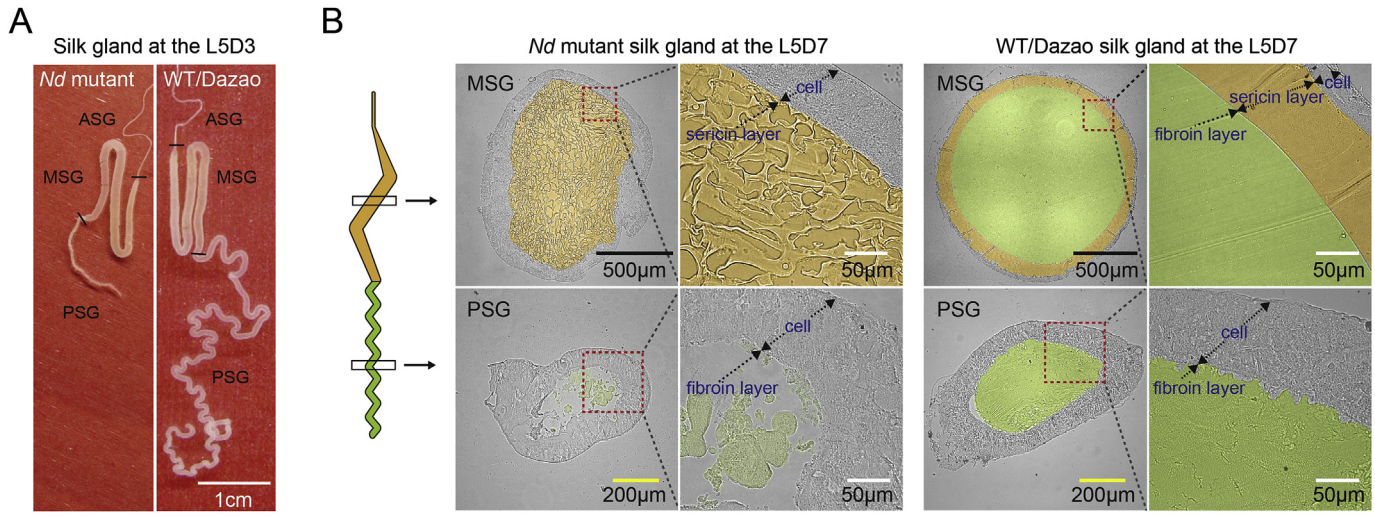

Fig. 3. Silk gland histomorphology and section observation. (A) Silk gland of *Nd* mutants and WT/Dazao at the L5D3. ASG, anterior silk gland; MSG, middle silk gland; PSG, posterior silk gland. (B) Silk gland cross-section observation of *Nd* mutants and WT/Dazao at the L5D7. Sericin layer was false-colored orange and fibroin layer was false-colored green in the silk gland lumen. (For interpretation of the references to color in this figure legend, the reader is referred to the Web version of this article.)

to 48.05% suggested a high confidence level for the RNA-Seq performed in this study (Table S1).

After filtering, 61.05%–74.14% of the clean reads were mapped to the silkworm genome (Xia et al., 2004) using TopHat with 59.25%–72.67% of the reads in the four libraries being uniquely mapped to the silkworm genome. Based on the expected number of Fragments Per Kilobase of transcript sequence per Millions base pairs sequenced (FPKM) method (Trapnell et al., 2012), the number of unigenes expressed in the *Nd*-PSG and WT-PSG were 11,090 and 10,721 respectively (Table S2). Pearson correlation analysis showed that the coefficient of variation (R^2) between the *Nd*-PSG and WT-PSG was 0.764–0.805 (Fig. 5A), suggesting that a wide differential gene expression between the *Nd*-PSG and WT-PSG.

An adjusted *P* value (*P*adj) ≤ 0.005 and a $\log_2$ (Fold change) ≥ 1 were set as the criteria for screening differentially expressed genes (DEGs): 2178 DEGs (1254 up-regulated and 924 down-regulated) were identified (Fig. 5B, Table S3). Mapping of the DEGs to the reference canonical pathways in the Kyoto Encyclopedia of Genes and Genomes (KEGG) showed significant enrichment of 134 pathways (Table S4). We analyzed the top 20% pathways and found significant enrichment of four pathways related to cellular stress responses (protein processing in ER, lysosomes, endocytosis, and phagosomes), and three pathways related to neurodegenerative diseases (Huntington's disease, Alzheimer's disease, and Parkinson's disease) involved in ameliorating risk to cells because of damaged proteins (Ellgaard and Helenius, 2003) (Fig. 5C). These results imply that *Nd*-PSG cells initiate cellular stress responses to mutant FibH.

3.6. Silk protein coding genes and silk gland transcription factors

The silk glands are responsible for synthesizing and secreting silk protein. In *Nd*-PSG, fibroin proteins were expressed but not secreted

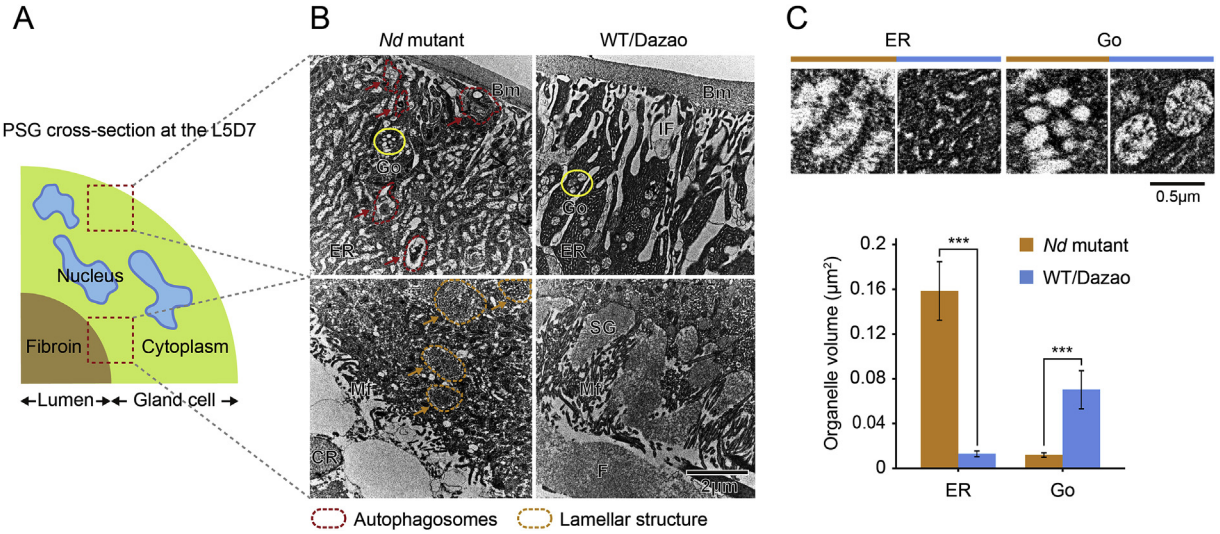

Fig. 4. Secretion deficiency of fibroin in *Nd*-PSG. (A) Schematic representation of the PSG cross-section. Red dotted boxes indicate the region observed by TEM. (B) Transmission electron microscopy (TEM) observation of the *Nd*-PSG and WT-PSG cells. Red arrows/circles, autophagosomes; orange arrows/circles, lamellar structure, a precursor of an autophagosome; yellow circles, Golgi apparatus (Go); ER, endoplasmic reticulum; Bm, basement membrane; IF, basal infolding; Mf, microfilaments; CR, cytoplasmic residue; SG, secretory globules; F, fibroin fibers. (C) Comparison of the lumen volume of ER and Go between the *Nd*-PSG and WT-PSG. Values are means ± SD (n = 3). Asterisks represent significant difference determined by Student's *t*-test at *P* value < 0.001 (***). (For interpretation of the references to color in this figure legend, the reader is referred to the Web version of this article.)

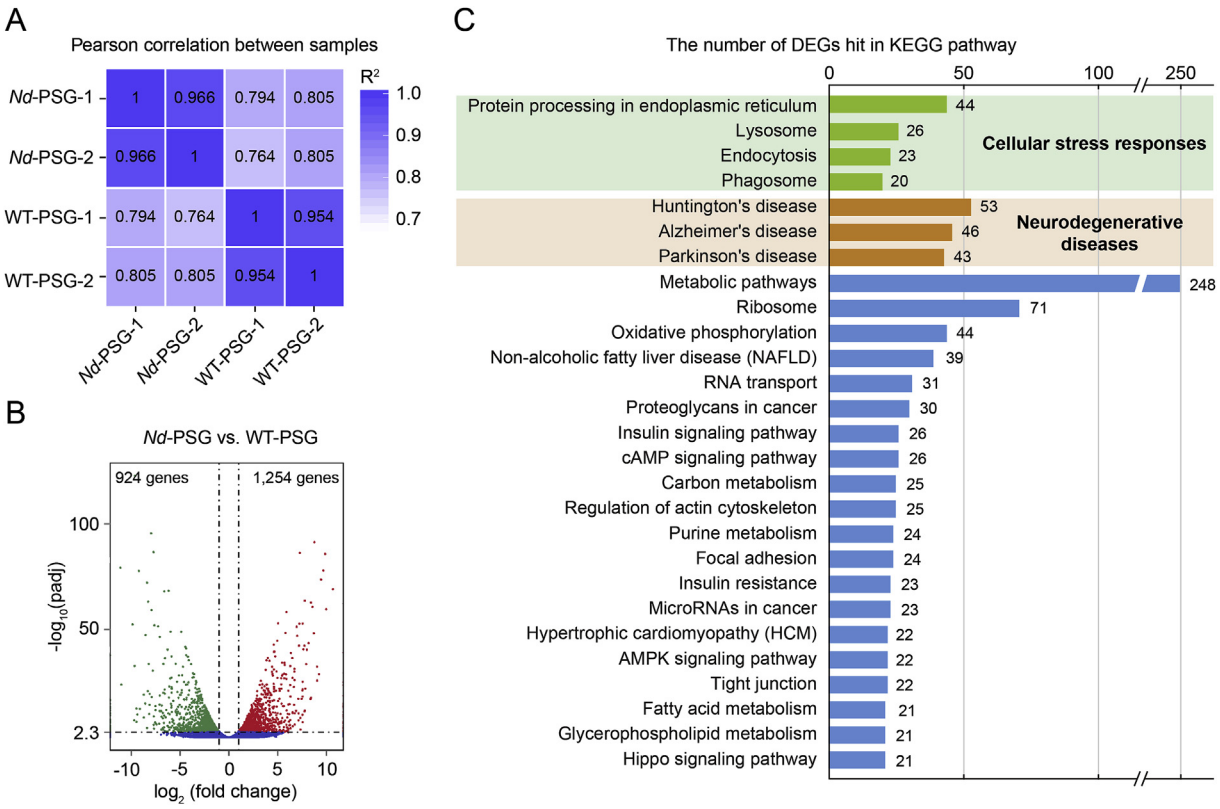

Fig. 5. Transcriptome analysis of the *Nd*-PSG and WT-PSG. (A) Pearson correlation analysis between *Nd*-PSG and WT-PSG at the L5D3. R^2, the square of Pearson's correlation coefficient. (B) DEGs number between the *Nd*-PSG and WT-PSG. Red dots indicate significantly up-regulated genes, green dots indicate significantly down-regulated genes, and blue dots indicate genes not significantly up or down-regulated. Log_2 (fold change) ≥ 1 and *P*adj value < 0.005 were set as the criteria for screening DEGs. (C) Kyoto Encyclopedia of Genes and Genomes (KEGG) enrichment analysis of the DEGs found between the *Nd*-PSG and WT-PSG. Orange, enriched pathway in degenerative disease; blue, enriched pathway in cellular stress responses. (For interpretation of the references to color in this figure legend, the reader is referred to the Web version of this article.)

Table 1
Expression levels of silk protein coding genes and silk gland transcription factors.

Gene_ID		*Nd* mutant-PSG	WT/Dazao-PSG	log_2 (fold change)
Silk protein coding genes				
FibH	*BGIBMGA005111*	48,742.33	5426048.81	−6.80 *
FibL	*BGIBMGA009393*	290,160.73	1838253.36	−2.66 *
P25/fhx	*BGIBMGA001347*	49,006.66	396,590.85	−3.02 *
Sericin1	*BGIBMGA001793*	329.98	548.78	–
Sericin2	*BGIBMGA011901*	742.76	2436.33	–
Sericin3	*BGIBMGA012002*	2.46	3.20	–
Silk gland transcription factors				
SGF-1/Fkh	*BGIBMGA005101*	836.21	574.45	+
SGF-2 (Awh)	*BGIBMGA003888*	35.73	190.50	−2.41 *
SGF-2 (Lbd)	*BGIBMGA012202*	1433.66	1755.54	–
SGF-2 (Lcaf)	*BGIBMGA009565*	310.49	80.38	+1.95 *
SGF-3/POUM1	*BGIBMGA010868*	59.31	24.87	+
FMBP-1	*BGIBMGA002810*	143.24	129.48	+
Sage	*BGIBMGA005127*	2688.39	2404.59	+
Dimm	*BGIBMGA007303*	411.02	1351.41	–

The gene expression level was calculated by the FPKM method. The value of log_2 (fold change) was calculated by log_2 (Readcount_*Nd* mutant-PSG/ Readcount_ WT/Dazao-PSG). "+" represents up-regulation, and "-" represents down-regulation. "*" represents a differentially expressed gene (DEG), and only the ratio of those DEGs are given. SGF, silk gland factor; Awh, arrowhead; Lbd, LIM domain-binding protein; Lcaf, single-stranded DNA-binding protein; POU, Pituitary-Octamer-Unc transcription factor; FMBP, fibroin modulator binding protein.

from cell to lumen, and the amount of fibroin was decreased (Hu et al., 2019). Therefore, we analyzed the expression level of three fibroin genes (*FibH*, *FibL*, and *P25*) and three sericin genes (*Sericin1*, *Sericin2*, and *Sericin3*). The results showed a significantly down-regulated expression of fibroin genes in *Nd*-PSG, among which the mRNA level of *Nd-FibH* was less than one percent that of WT-*FibH* (Table 1), but still at the same level with housekeeping gene *Nd-Rpl3* (*BGIBMGA013567*) (Table S2). Next, the expression profiles of silk gland transcription factors involved in transcriptional regulation of silk genes were analyzed, such as *SGF-1/Fkh* (Mach et al., 1995), *SGF-2* (Ohno et al., 2013), *SGF-3/POUM1* (Kimoto et al., 2012), *FMBP-1* (Takiya et al., 1997), *Sage* (Zhao et al., 2014), and *Dimm* (Zhao et al., 2015). In *Nd*-PSG, the expression level of most of the silk gland transcription factors revealed no significant change (Table 1), except for an up-regulated SGF2 subunit (*Lcaf*) and a down-regulated SGF2 subunit (*Awh*), which might act as a counterbalance. These findings suggested that the down-regulation of the fibroin genes may not be controlled by silk gland transcription factors.

In addition, the expression patterns of the genes involved in the mRNA degradation pathway were analyzed, and most DEGs, such as *Ago1*, *Ago2*, *Ago3*, *Dicer1*, and *Dicer2*, were significantly up-regulated in *Nd*-PSG (Table S5). Thus, it is suggested that the mRNA degradation pathway was activated and correlated with fibroin mRNA degradation in *Nd*-PSG.

3.7. Genes involved in the cellular stress responses

Cells have to cope with protein damage in order to survive. To that end, they evolved the cellular stress responses, such as autophagy,

Table 2
Expression levels of the genes involved in the autophagy and apoptosis pathways.

Gene_ID			*Nd* mutant-PSG	WT/Dazao-PSG	log_2 (fold change)
Autophagy pathway					
Ubiquitin-like conjugation pathway	*ATG3*	*BGIBMGA003767*	682.76	565.35	+
	ATG4	*BGIBMGA004926*	301.96	296.71	+
	ATG5	*BGIBMGA007878*	140.35	225.26	–
	ATG7	*BGIBMGA001467*	307.13	295.99	+
	ATG8	*BGIBMGA011783*	4967.97	2372.18	+1.07 *
	ATG12	*BGIBMGA003954*	48.97	114.68	–
	ATG16	*BGIBMGA006504*	37.98	14.05	+
Signal transduction pathway	*PI3K–I*	*BGIBMGA010561*	343.30	139.37	+
	Pdk1	*BGIBMGA011755*	551.50	117.63	+2.23 *
	Akt/Pkb	*BGIBMGA014132*	42.55	17.36	+
	Tsc1	*BGIBMGA005845*	1663.55	1531.10	+
	Tsc2	*BGIBMGA005686*	1385.51	943.86	+
	Rheb	*BGIBMGA006257*	703.71	478.64	+
	AMPK	*BGIBMGA013139*	174.88	95.11	+
	TOR	*BGIBMGA008952*	484.81	299.01	+
	Tap42	*BGIBMGA013517*	138.03	55.90	+
	Pp2A	*BGIBMGA010831*	280.36	136.77	+
	P70s6K	*BGIBMGA011088*	153.11	190.25	–
	PI3K-III	*BGIBMGA007158*	164.45	71.48	+
	ATG6	*BGIBMGA000092*	357.74	184.84	+
Others	*Hsc73*	*BGIBMGA002381*	216,760.51	249,982.03	–
	ATG1	*BGIBMGA011986*	751.51	1923.03	–
	ATG9	*BGIBMGA012307*	163.89	25.16	+2.70 *
	ATG18	*BGIBMGA007298*	194.97	205.76	–
Apoptosis pathway					
Caspase-1		*BGIBMGA006946*	157.81	87.49	+
Caspase-4		*BGIBMGA004420*	1.64	1.28	+
Dredd		*BGIBMGA006726*	172.55	147.62	+
Dronc		*BGIBMGA002841*	333.90	325.59	+
ICE		*BGIBMGA006131*	75.65	1.28	+5.88 *

The gene expression level was calculated by the FPKM method. The value of log_2 (fold change) was calculated by log_2 (Readcount_*Nd* mutant-PSG/Readcount_ WT/Dazao-PSG). "+" represents up-regulation, and "-" represents down-regulation. "*" represents a differentially expressed gene (DEG), and only the ratio of those DEGs are given. ATG, autophagy related protein; PI3K, phosphatidylinositol 3-kinase; Pdk, phosphoinositide-dependent protein kinase; Akt/Pkb, protein kinase B; Tsc, tuberous sclerosis complex; Rheb, Ras homolog enriched in brain; AMPK, AMP-activated protein kinase; TOR, target of rapamycin; Tap, two A-associated protein; Pp2A, protein phosphatase 2A; P70s6K, ribosomal protein S6 kinase; Hsc, heat shock cognate protein; ICE, interleukin-1 beta converting enzyme.

protein hydrolysis (ubiquitin-proteasome system), and heat shock response (Buchberger et al., 2010). We analyzed the expression level of the genes involved in the autophagy pathway. *ATG8*, a marker gene to indicate the autophagic activity (Zhang et al., 2009), *Pdk1*, and *ATG9* were significantly up-regulated in *Nd*-PSG (Table 2). The expression level analysis of the genes involved in the apoptosis pathway revealed that *ICE*, coding for a cysteine-type endopeptidase, was also significantly up-regulated in *Nd*-PSG (Table 2). These findings were consistent with the autophagosomes and lamellar structures in the cytoplasm of *Nd*-PSG observed by TEM (Fig. 4B), suggesting that the autophagy and the apoptosis pathways were activated to initiate autophagosome and lysosome formation in *Nd*-PSG.

Then, the genes that are involved in the ubiquitin-proteasome system (UPS) and heat shock response were analyzed. Remarkably, seven ubiquitin-protein ligase (*E3*) and five other ubiquitin hydrolase (*E other*) genes were significantly up-regulated in *Nd*-PSG (Table 3). Twelve heat shock proteins were significantly up-regulated in *Nd*-PSG (Table 3), and interestingly, most were small heat shock proteins. These results suggested that the UPS pathway and heat shock response were actively involved in the elimination of protein damage caused by mutant FibH in *Nd*-PSG.

3.8. Expression profiles of fibroin genes and DEGs involved in the cellular stress responses at three typical larval instars

To further investigate the molecular features of developmental defects in *Nd*-PSG during silk gland growth, as well as to validate RNA-Seq data, we performed the expression profiles of fibroin genes (*FibH*, *FibL*, and *P25*) and the DEGs involved in the cellular stress responses (autophagy (*ATG8*), ubiquitin-proteasome system (*E3* and *E other*), and heat shock response (*Hsp19.9* and *Hsp70*)) in PSG at three typical larval instars: the neonatal larval stage with no nuclear ramification; the L4D1, in which nuclear ramifications appeared; and the L5D3 of conspicuous nuclear ramifications. In these stages, the expression levels of fibroin genes in *Nd*-PSG were significantly lower than in WT-PSG. When the mutant *FibH* expression increased at the L4D1 and L5D3, the *ATG8*, *E3*, *E other*, *Hsp19.9*, and *Hsp70* expression levels in *Nd*-PSG were significantly higher than in WT-PSG (Fig. 6). These results suggested that cellular stress responses were enhanced with the increase in mutant *FibH*.

4. Discussion

The *Nd* mutant is a fibroin-deficient genetic resource that has been widely used to study silk gland development and fibroin synthesis, and the *Nd* locus (0.0 cM) has become a ubiquitous twenty-fifth chromosomal marker used by *Bombyx* geneticists to follow and track mutations (Hu et al., 2019). Here, we presented histomorphology and transcriptome analyses of the silk gland between *Nd* mutant and WT/Dazao during the larval stage. Our results revealed several developmental defects in *Nd*-PSG and the DEGs involved in the pathways conferring the drastic morphological and physiological differences between *Nd*-PSG and WT-PSG, further expanding our knowledge regarding silk gland growth and fibroin secretion of silkworm larva.

The silk gland is essentially a tube comprising large polyploid cells, each with an extremely ramified nucleus containing numerous nucleoli (Yukuhiro et al., 2016). Ramification considerably enlarges the nuclear surface and apparently facilitates the transfer of materials related to the silk synthesis between the nucleus and cytoplasm (Akai, 1983). Nuclear staining indicated that nuclear ramification developed gradually as the

Table 3
Differentially expressed genes involved in the protein proteolytic pathway and heat shock response.

Gene_ID		*Nd* mutant-PSG	WT/Dazao-PSG	$\log_2$ (fold change)	Gene description
Protein proteolytic pathway					
E2	*BGIBMGA005425*	1798.73	3761.63	−1.06 *	Ubiquitin-conjugating enzyme E2
	BGIBMGA007432	148.07	390.49	−1.40 *	Ubiquitin-conjugating enzyme E2
	BGIBMGA011117	472.66	1283.56	−1.44 *	Ubiquitin-fold modifier-conjugating enzyme 1
E3	*BGIBMGA009118*	443.78	1193.62	−1.43 *	Ubiquitin protein ligase
	BGIBMGA002878	421.06	102.15	+2.04 *	Ubiquitin-protein ligase E3
	BGIBMGA007076	459.12	94.47	+2.28 *	Ubiquitin-protein ligase E3
	BGIBMGA007519	6123.55	2945.49	+1.06 *	Ubiquitin-protein ligase E3
	BGIBMGA007893	777.12	332.14	+1.23 *	Ubiquitin ligase E3
	BGIBMGA009222	440.33	41.84	+3.40 *	Ubiquitin-protein ligase E3
	BGIBMGA010628	3196.35	1232.63	+1.37 *	Ubiquitin-protein ligase E3
	BGIBMGA014232	241.22	62.23	+1.95 *	Ubiquitin ligase E3
Others	*BGIBMGA002483*	1020.75	342.60	+1.58 *	Inactive ubiquitin carboxyl-terminal hydrolase 54
	BGIBMGA002507	482.01	143.78	+1.75 *	Ubiquitin carboxyl-terminal hydrolase 1
	BGIBMGA002759	1298.57	569.89	+1.19 *	Ubiquitin carboxyl-terminal hydrolase
	BGIBMGA006669	791.04	364.41	+1.12 *	Ubiquitin carboxyl-terminal hydrolase (Fragment)
	BGIBMGA007507	1589.66	472.64	+1.75 *	Ubiquitin carboxyl-terminal hydrolase
Heat shock response					
Hsp	*BGIBMGA001241*	1229.73	2787.82	−1.18 *	Heat shock protein
Hsp21.4	*BGIBMGA000944*	5792.24	21,913.37	−1.92 *	Heat shock protein 21.4
Small Hsp	*BGIBMGA005755*	5509.04	1061.97	+2.38 *	Small heat shock protein
Small Hsp	*BGIBMGA005780*	38.71	0.89	+5.44 *	Small heat shock protein
Hsp1	*BGIBMGA004103*	103.45	9.82	+3.40 *	Heat shock protein 1
Hsp19.5	*BGIBMGA013545*	20,162.25	28.75	+9.45 *	Heat shock protein 19.5
Hsp19.9	*BGIBMGA004540*	2847.41	794.34	+1.84 *	Heat shock protein 19.9
Hsp20.4	*BGIBMGA004541*	406.53	32.09	+3.66 *	Heat shock protein 20.4
Hsp20.8	*BGIBMGA004605*	1166.15	102.15	+3.51 *	Heat shock protein 20.8
Hsp22.2	*BGIBMGA004630*	679.95	47.68	+3.83 *	Small heat shock protein 22.2
Hsp23.7	*BGIBMGA004515*	35,682.20	68.14	+9.03 *	Heat shock protein 23.7
Hsp33.6	*BGIBMGA005823*	99.66	17.54	+2.51 *	Small heat shock protein 33.6
Hsp70	*BGIBMGA007950*	138,047.37	14,229.22	+3.28 *	Heat shock protein 70 cognate
Hsp70	*BGIBMGA014536*	38.75	1.53	+4.66 *	Heat shock protein 70

The gene expression level was calculated by the FPKM method. The value of $\log_2$ (fold change) was calculated by $\log_2$ (Readcount_*Nd* mutant-PSG/Readcount_ WT/Dazao-PSG). "+" represents up-regulation, and "-" represents down-regulation. "*" represents a differentially expressed gene (DEG).

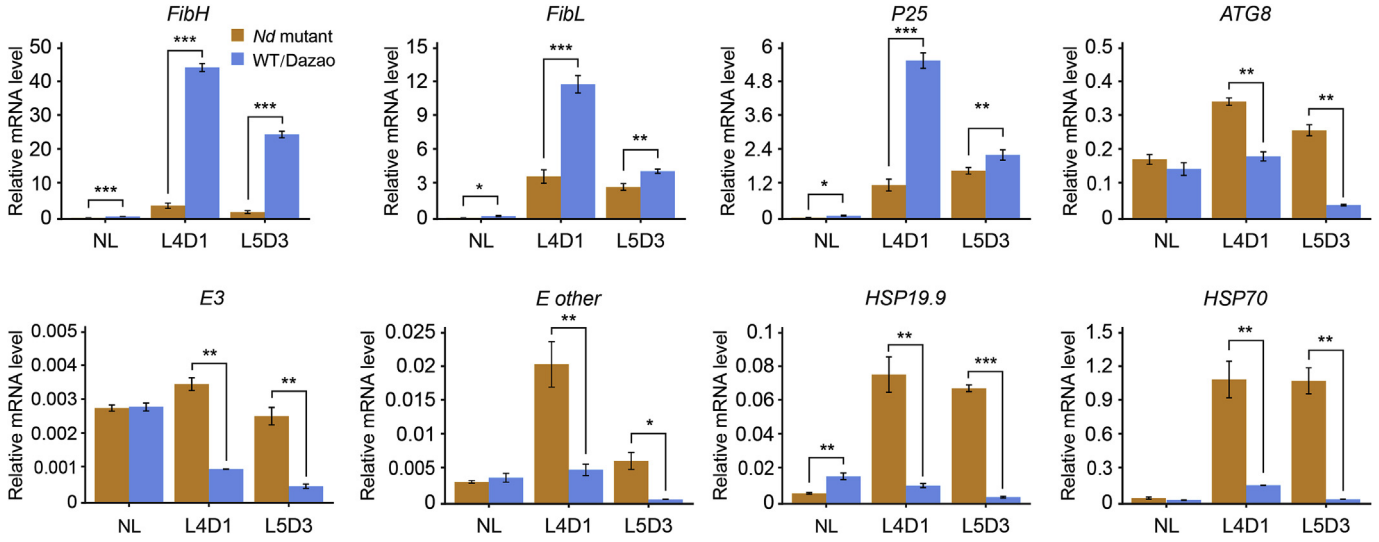

Fig. 6. Expression profiles of fibroin genes and DEGs at three typical larval instars. Relative mRNA levels of fibroin genes (*FibH*, *FibL*, and *P25*) and the DEGs involved in the cellular stress responses (autophagy (*ATG8*), ubiquitin-proteasome system (*E3* and *E other*), and heat shock response (*Hsp19.9* and *Hsp70*)) at the NL, L4D1, and L5D3. The silkworm housekeeping gene *ribosomal protein L3* (*Rpl3*) expression was used as a control. Values are means ± SD (n = 3). NL indicates the neonatal larval stage. Asterisks represent significant differences determined by a Student's *t*-test at *P* value < 0.01 (**), *P* value < 0.001 (***).

larvae grow and reached a conspicuous size at the fifth instar (Fig. 2A and B). Notably, we observed that, in the first half of the larval stage (before L4D1), the nuclear ramification of *Nd*-PSG and WT-PSG underwent similar development, while in the last half (after the L4D1), the difference between the two strains increased (Fig. 2B), which were consistent with the development trend of the PSG length between *Nd*-PSG and WT-PSG (Fig. 1A and B). In addition, *FibH* expression at the L4D1 was almost twice the level of that at the L5D3 (Fig. 6), a period with the highest rate of mRNA synthesis at the fifth instar (Kimura et al., 1985; Maekawa and Suzuki, 1980). Thus, these results imply that the L4D1 represents a key stage during silk gland development.

Silk is efficiently secreted from the silk gland, stored in their lumen, and converted into a solid filament during spinning to construct cocoons for larvae pupation. An intact fibroin unit (FibH, FibL, and P25 at

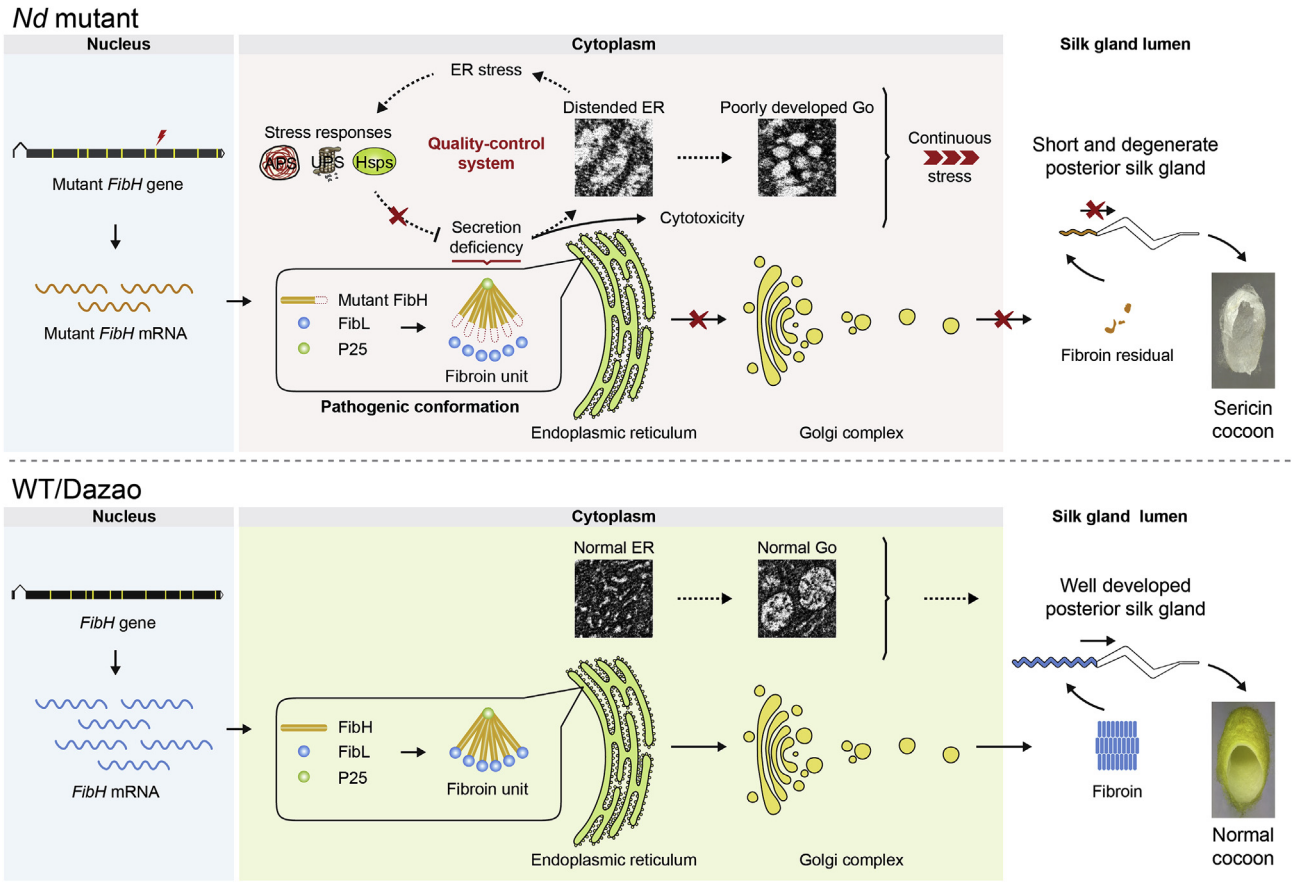

Fig. 7. A model describing the *Nd* mutation mechanism. In the WT-PSG, structural intact FibH assembled into fibroin unit with FibL and P25, which was successfully secreted into PSG lumen through intracellular transport. However, in the *Nd*-PSG, mutant *FibH* encodes a truncated FibH, which might misassemble into a pathogenic conformation in ER, resulting in cellular stress responses (autophagy, protein hydrolysis, and heat shock response). With larva growth, *Nd*-PSG was under continuous stress, which eventually presented gland atrophy. The solid arrow indicates direct processes, dotted arrow indirect processes, the red-cross indicates the process was blocked, and three red line arrowheads indicate continuous stress responses. Go, Golgi apparatus; ER, endoplasmic reticulum; APS, autophagosome; UPS, ubiquitin-proteasome system; Hsps, heat shock proteins. (For interpretation of the references to color in this figure legend, the reader is referred to the Web version of this article.)

a molar ratio of 6:6:1) is essential for secretion of silk fibroin from the PSG cells into the lumen (Aramwit et al., 2012; Inoue et al., 2000). Our previous results showed that mutant FibH was blocked in *Nd*-PSG cell (Hu et al., 2019). In this study, TEM observations showed that proteins were accumulated in the ER and not secreted from PSG cells (Fig. 4B and C). Thus we speculated that mutant FibH obstructed the ER and blocked intracellular transport in *Nd*-PSG. The *Nd*-ER were distended with accumulated fibroin protein, and the *Nd*-Go were poorly developed (Fig. 4C). The ER is an essential intracellular organelle responsible for the synthesis, folding, and trafficking of secretory proteins (Ryoo, 2016; Xiang et al., 2017), and the Go is an organelle for processing newly synthesized proteins (received from the ER) moving through the secretory pathway (Gao et al., 2014; Sengupta and Linstedt, 2011). Thus, in ER, the truncated FibH might lead to a mis-assembled fibroin unit (damaged protein), which was not able to be transported to Go and perturbed cellular homeostasis, implying that ER was the cellular site where an elementary unit of fibroin was assembled.

In cells, the accumulation of damaged proteins, resulting from mutation/misfolding/aggregation, can perturb cellular homeostasis and endanger survival under severe stress conditions (Buchberger et al., 2010; Ellgaard and Helenius, 2003). Parallel to attempts to repair or degrade acutely damaged proteins, stressed cells undergo adaptive responses aimed at reducing protein damage by a decrease in global protein translation and an increase in molecular chaperones and proteins of proteolytic systems (Gawron, 2016; Goldberg, 2003; Stefani and Dobson, 2003). In the present study, fibroin secretion was blocked in the ER of *Nd*-PSG (Fig. 4C), four genes involved in autophagy and apoptosis pathways, twelve genes involved in protein proteolytic pathway, and twelve genes involved in heat shock response were significantly up-regulated in the PSG (Tables 2 and 3). Besides, four KEGG pathways (protein processing in ER, lysosomes, endocytosis, and phagosomes) were significantly enriched by DEGs. These results suggested that cellular stress responses were activated in *Nd*-PSG. Interestingly, KEGG pathway analysis also showed that DEGs in *Nd*-PSG were enriched in neurodegenerative diseases (Huntington's disease, Alzheimer's disease, and Parkinson's disease) associated with the aggregation of misfolded proteins (polyglutamine tract (Bates et al., 2015), beta-amyloid (Giacobini and Gold, 2013), and alpha-synuclein (Irwin et al., 2013), respectively) (Fig. 5C). Similarly, the mutant FibH is an aggregation of a single repetitive unit (Hu et al., 2019). In addition, following the accumulation of mutant FibH in *Nd*-PSG cells during larval growth, a short and degenerate PSG was generated in the *Nd* mutant (Fig. 1A and B). A previous study based on quantitative proteomic analysis of the naked pupa strain (ZB) presented a consistent result of neurodegenerative diseases in KEGG pathway analysis (Wang et al., 2014). Therefore, we speculate that the secretion-deficient FibH is cytotoxic, and the pathogenic effects of aggregated repetitive regions in mutant FibH that were accompanied by cellular stress responses and PSG degeneration in *Nd* mutants are similar to those in neurodegenerative diseases.

Based on our results, we propose a model describing the mechanisms underlying the effects of the *Nd* mutation (Fig. 7): The *Nd-FibH*

encodes a truncated FibH, which may assemble into an incorrect fibroin unit, thus obstructing the ER. This induces ER stress and triggers cellular stress responses to decrease the production of the mutant protein. In addition, high-molecular weight/repetitive mutant FibH accumulates during larval development; the accumulated protein is difficult to hydrolyze, which leads to distention of the endoplasmic reticula and poor development of the Golgi apparatus. Continuous cellular stress during larval growth may result in a gland atrophy of the PSG, resulting in a short gland, low DNA copy number, and low *FibH* expression level; moreover, fibroin may not be secreted into the PSG lumen, transported into the MSG lumen, or spun as silk to form a sericin cocoon.

Data availability

All relevant data and material are available from the authors. Raw data presented in this paper have been deposited in the NCBI Short Read Archive (http://www.ncbi.nlm.nih.gov/sra/) under the following accession numbers: SRR6002262, SRR6002263, SRR6002264, and SRR6002265.

Acknowledgments

We thank Dr. Chun Liu (Southwest University, China) and Dr. Tingcai Cheng (Southwest University, China) for comments and suggestions on the manuscript. This work was supported by grants from the key program of the National Natural Science Foundation of China (31530071), the Chongqing Research Program of Basic Research and Frontier Technology (cstc2017jcyjAX0090), and the Chongqing Special Postdoctoral Science Foundation (XmT2018060).

Appendix A. Supplementary data

Supplementary data to this article can be found online at https://doi.org/10.1016/j.ibmb.2019.05.010.

References

Akai, H., 1979. Hormonal control of silk production in silkworm, *Bombyx mori*. Jpn. Agric. Res. Q. 13, 116–122.
Akai, H., 1983. The structure and ultrastructure of the silk gland. Experientia 39, 443–449.
Anders, S., Huber, W., 2010. Differential expression analysis for sequence count data. Genome Biol. 11, R106.
Anders, S., Pyl, P.T., Huber, W., 2015. HTSeq–a Python framework to work with high-throughput sequencing data. Bioinformatics 31, 166–169.
Andersson, M., Johansson, J., Rising, A., 2016. Silk spinning in silkworms and spiders. Int. J. Mol. Sci. 17.
Aramwit, P., Siritientong, T., Srichana, T., 2012. Potential applications of silk sericin, a natural protein from textile industry by-products. Waste Manag. Res. : the journal of the International Solid Wastes and Public Cleansing Association, ISWA 30, 217–224.
Asakura, T., Umemura, K., Nakazawa, Y., Hirose, H., Higham, J., Knight, D., 2007. Some observations on the structure and function of the spinning apparatus in the silkworm *Bombyx mori*. Biomacromolecules 8, 175–181.
Bates, G.P., Dorsey, R., Gusella, J.F., Hayden, M.R., Kay, C., Leavitt, B.R., Nance, M., Ross, C.A., Scahill, R.I., Wetzel, R., 2015. Huntington's disease. Nature reviews Disease primers 1.
Buchberger, A., Bukau, B., Sommer, T., 2010. Protein quality control in the cytosol and the endoplasmic reticulum: brothers in arms. Mol. Cell 40, 238–252.
Craig, C.L., 1997. Evolution of arthropod silks. Annu. Rev. Entomol. 42, 231–267.
Dhawan, S., Gopinathan, K.P., 2003. Expression profiling of homeobox genes in silk gland development in the mulberry silkworm *Bombyx mori*. Dev. Gene. Evol. 213, 523–533.
Ellgaard, L., Helenius, A., 2003. Quality control in the endoplasmic reticulum. Nat. Rev. Mol. Cell Biol. 4, 181–191.
Franzetti, E., Huang, Z.J., Shi, Y.X., Xie, K., Deng, X.J., Li, J.P., Li, Q.R., Yang, W.Y., Zeng, W.N., Casartelli, M., Deng, H.M., Cappellozza, S., Grimaldi, A., Xia, Q., Feng, Q., Cao, Y., Tettamanti, G., 2012. Autophagy precedes apoptosis during the remodeling of silkworm larval midgut. Apoptosis : Int. J. Programm. Cell Death 17, 305–324.
Gao, C., Cai, Y., Wang, Y., Kang, B.H., Aniento, F., Robinson, D.G., Jiang, L., 2014. Retention mechanisms for ER and Golgi membrane proteins. Trends Plant Sci. 19, 508–515.
Gawron, K., 2016. Endoplasmic reticulum stress in chondrodysplasias caused by mutations in collagen types II and X. Cell Stress & Chaperones 21, 943–958.
Giacobini, E., Gold, G., 2013. Alzheimer disease therapy—moving from amyloid-β to tau. Nat. Rev. Neurol. 9, 677–686.
Goldberg, A.L., 2003. Protein degradation and protection against misfolded or damaged proteins. Nature 426, 895–899.
Goldsmith, M.R., Shimada, T., Abe, H., 2005. The genetics and genomics of the silkworm, *Bombyx mori*. Annu. Rev. Entomol. 50, 71–100.
Hu, W., Liu, C., Cheng, T., Li, W., Wang, N., Xia, Q., 2016. Histomorphometric and transcriptomic features characterize silk glands' development during the molt to intermolt transition process in silkworm. Insect Biochem. Mol. Biol. 76, 95–108.
Hu, W., Lu, W., Wei, L., Zhang, Y., Xia, Q., 2019. Molecular nature of dominant naked pupa mutation reveals novel insights into silk production in Bombyx mori. Insect Biochem. Mol. Biol. 109, 52–62.
Inoue, S., Tanaka, K., Arisaka, F., Kimura, S., Ohtomo, K., Mizuno, S., 2000. Silk fibroin of *Bombyx mori* is secreted, assembling a high molecular mass elementary unit consisting of H-chain, L-chain, and P25, with a 6:6:1 molar ratio. J. Biol. Chem. 275, 40517–40528.
Irwin, D.J., Lee, V.M.-Y., Trojanowski, J.Q., 2013. Parkinson's disease dementia: convergence of α-synuclein, tau and amyloid-β pathologies. Nat. Rev. Neurosci. 14, 626–636.
Kanehisa, M., Goto, S., 2000. KEGG: kyoto encyclopedia of genes and genomes. Nucleic Acids Res. 28, 27–30.
Kimoto, M., Kitagawa, T., Kobayashi, I., Nakata, T., Kuroiwa, A., Takiya, S., 2012. Inhibition of the binding of MSG-intermolt-specific complex, MIC, to the sericin-1 gene promoter and sericin-1 gene expression by POU-M1/SGF-3. Dev. Gene. Evol. 222, 351–359.
Kimura, K., Oyama, F., Ueda, H., Mizuno, S., Shimura, K., 1985. Molecular cloning of the fibroin light chain complementary DNA and its use in the study of the expression of the light chain gene in the posterior silk gland of *Bombyx mori*. Experientia 41, 1167–1171.
Kokubo, H., Takiya, S., Mach, V., Suzuki, Y., 1996. Spatial and temporal expression pattern of *Bombyx* fork head/SGF-1 gene in embryogenesis. Dev. Gene. Evol. 206, 80–85.
Kokubo, H., Ueno, K., Amanai, K., Suzuki, Y., 1997. Involvement of the *Bombyx Scr* gene in development of the embryonic silk gland. Dev. Biol. 186, 46–57.
Liu, X., Zhang, K., 2014. Silk fiber—molecular formation mechanism, structure-property relationship and advanced applications. Oligomerization Chem. Biol. Compd. 3.
Ma, L., Xu, H., Zhu, J., Ma, S., Liu, Y., Jiang, R.J., Xia, Q., Li, S., 2011. Ras1(CA) overexpression in the posterior silk gland improves silk yield. Cell Res. 21, 934–943.
Ma, S., Shi, R., Wang, X., Liu, Y., Chang, J., Gao, J., Lu, W., Zhang, J., Zhao, P., Xia, Q., 2014. Genome editing of *BmFib-H* gene provides an empty *Bombyx mori* silk gland for a highly efficient bioreactor. Sci. Rep. 4, 6867.
Mach, V., Takiya, S., Ohno, K., Handa, H., Imai, T., Suzuki, Y., 1995. Silk gland factor-1 involved in the regulation of *Bombyx sericin-1* gene contains fork head motif. J. Biol. Chem. 270, 9340–9346.
Maekawa, H., Suzuki, Y., 1980. Repeated turn-off and turn-on of fibroin gene transcription during silk gland development of *Bombyx mori*. Dev. Biol. 78, 394–406.
Mori, K., Tanaka, K., Kikuchi, Y., Waga, M., Waga, S., Mizuno, S., 1995. Production of a chimeric fibroin light-chain polypeptide in a fibroin secretion-deficient naked pupa mutant of the silkworm *Bombyx mori*. J. Mol. Biol. 251, 217–228.
Morimoto, T., Matsuura, S., Nagata, S., Tashiro, Y., 1968. Studies on the posterior silk gland of the silkworm, *Bombyx mori*: III. Ultrastructural changes of posterior silk gland cells in the fourth larval instar. J. Cell. Biol. 38, 604–614.
Nakano, Y., 1951. Physiological, anatomical and genetical studies on the “Naked” silkworm pupa. J. Seric. Sci. Jpn. 20, 232–248.
Ohno, K., Sawada, J., Takiya, S., Kimoto, M., Matsumoto, A., Tsubota, T., Uchino, K., Hui, C.C., Sezutsu, H., Handa, H., Suzuki, Y., 2013. Silk gland factor-2, involved in fibroin gene transcription, consists of LIM homeodomain, LIM-interacting, and single-stranded DNA-binding proteins. J. Biol. Chem. 288, 31581–31591.
Omenetto, F.G., Kaplan, D.L., 2010. New opportunities for an ancient material. Science 329, 528–531.
Perdrix-Gillot, S., 1979. DNA synthesis and endomitoses in the giant nuclci of the silkgland of *Bombyx mori*. Biochimie 61, 171–204.
Ryoo, H.D., 2016. Long and short (timeframe) of endoplasmic reticulum stress-induced cell death. FEBS J. 283, 3718–3722.
Sehnal, F., Akai, H., 1990. Insect silk glands: their types, development and function, and effects of environmental factors and morphogenetic hormones on them. Int. J. Insect Morphol. Embryol. 19, 79–132.
Sengupta, D., Linstedt, A.D., 2011. Control of organelle size: the Golgi complex. Annu. Rev. Cell Dev. Biol. 27, 57–77.
Stefani, M., Dobson, C.M., 2003. Protein aggregation and aggregate toxicity: new insights into protein folding, misfolding diseases and biological evolution. J. Mol. Med. 81, 678–699.
Sutherland, T.D., Young, J.H., Weisman, S., Hayashi, C.Y., Merritt, D.J., 2010. Insect silk: one name, many materials. Annu. Rev. Entomol. 55, 171–188.
Takei, F., Kikuchi, Y., Kikuchi, A., Mizuno, S., Shimura, K., 1987. Further evidence for importance of the subunit combination of silk fibroin in its efficient secretion from the posterior silk gland cells. J. Cell. Biol. 105, 175–180.
Takiya, S., Kokubo, H., Suzuki, Y., 1997. Transcriptional regulatory elements in the upstream and intron of the fibroin gene bind three specific factors POU-M1, Bm Fkh and FMBP-1. Biochem. J. 321 (Pt 3), 645–653.
Trapnell, C., Roberts, A., Goff, L., Pertea, G., Kim, D., Kelley, D.R., Pimentel, H., Salzberg, S.L., Rinn, J.L., Pachter, L., 2012. Differential gene and transcript expression analysis of RNA-seq experiments with TopHat and Cufflinks. Nat. Protoc. 7, 562–578.
Trapnell, C., Williams, B.A., Pertea, G., Mortazavi, A., Kwan, G., van Baren, M.J., Salzberg, S.L., Wold, B.J., Pachter, L., 2010. Transcript assembly and quantification by RNA-Seq reveals unannotated transcripts and isoform switching during cell differentiation. Nat. Biotechnol. 28, 511–515.
Vepari, C., Kaplan, D.L., 2007. Silk as a biomaterial. Prog. Polym. Sci. 32, 991–1007.

Wang, J., Xia, Q., He, X., Dai, M., Ruan, J., Chen, J., Yu, G., Yuan, H., Hu, Y., Li, R., Feng, T., Ye, C., Lu, C., Wang, J., Li, S., Wong, G.K., Yang, H., Wang, J., Xiang, Z., Zhou, Z., Yu, J., 2005. SilkDB: a knowledgebase for silkworm biology and genomics. Nucleic Acids Res. 33, D399–D402.

Wang, S.H., You, Z.Y., Ye, L.P., Che, J., Qian, Q., Nanjo, Y., Komatsu, S., Zhong, B.X., 2014. Quantitative proteomic and transcriptomic analyses of molecular mechanisms associated with low silk production in silkworm *Bombyx mori*. J. Proteome Res. 13, 735–751.

Wang, X., Zhao, P., Li, Y., Yi, Q., Ma, S., Xie, K., Chen, H., Xia, Q., 2015. Modifying the mechanical properties of silk fiber by genetically disrupting the ionic environment for silk formation. Biomacromolecules 16, 3119–3125.

Xia, Q., Li, S., Feng, Q., 2014. Advances in silkworm studies accelerated by the genome sequencing of *Bombyx mori*. Annu. Rev. Entomol. 59, 513–536.

Xia, Q., Zhou, Z., Lu, C., Cheng, D., Dai, F., Li, B., Zhao, P., Zha, X., Cheng, T., Chai, C., Pan, G., Xu, J., Liu, C., Lin, Y., Qian, J., Hou, Y., Wu, Z., Li, G., Pan, M., Li, C., Shen, Y., Lan, X., Yuan, L., Li, T., Xu, H., Yang, G., Wan, Y., Zhu, Y., Yu, M., Shen, W., Wu, D., Xiang, Z., Yu, J., Wang, J., Li, R., Shi, J., Li, H., Li, G., Su, J., Wang, X., Li, G., Zhang, Z., Wu, Q., Li, J., Zhang, Q., Wei, N., Xu, J., Sun, H., Dong, L., Liu, D., Zhao, S., Zhao, X., Meng, Q., Lan, F., Huang, X., Li, Y., Fang, L., Li, C., Li, D., Sun, Y., Zhang, Z., Yang, Z., Huang, Y., Xi, Y., Qi, Q., He, D., Huang, H., Zhang, X., Wang, Z., Li, W., Cao, Y., Yu, Y., Yu, H., Li, J., Ye, J., Chen, H., Zhou, Y., Liu, B., Wang, J., Ye, J., Ji, H., Li, S., Ni, P., Zhang, J., Zhang, Y., Zheng, H., Mao, B., Wang, W., Ye, C., Li, S., Wang, J., Wong, G.K., Yang, H., Biology Analysis, G., 2004. A draft sequence for the genome of the domesticated silkworm (*Bombyx mori*). Science 306, 1937–1940.

Xiang, C., Wang, Y., Zhang, H., Han, F., 2017. The role of endoplasmic reticulum stress in neurodegenerative disease. Apoptosis : Int. J. Programm. Cell Death 22, 1–26.

Xie, C., Mao, X., Huang, J., Ding, Y., Wu, J., Dong, S., Kong, L., Gao, G., Li, C.Y., Wei, L., 2011. KOBAS 2.0: a web server for annotation and identification of enriched pathways and diseases. Nucleic Acids Res. 39, W316–W322.

Xie, K., Tian, L., Guo, X., Li, K., Li, J., Deng, X., Li, Q., Xia, Q., Zhong, Y., Huang, Z., Liu, J., Li, S., Yang, W., Cao, Y., 2016. BmATG5 and BmATG6 mediate apoptosis following autophagy induced by 20-hydroxyecdysone or starvation. Autophagy 12, 381–396.

Yukuhiro, K., Sezutsu, H., Tsubota, T., Takasu, Y., Kameda, T., Yonemura, N., 2016. Insect Silks and Cocoons: Structural and Molecular Aspects, Extracellular Composite Matrices in Arthropods. Springer, pp. 515–555.

Zhang, X., Hu, Z.Y., Li, W.F., Li, Q.R., Deng, X.J., Yang, W.Y., Cao, Y., Zhou, C.Z., 2009. Systematic cloning and analysis of autophagy-related genes from the silkworm *Bombyx mori*. BMC Mol. Biol. 10, 50.

Zhao, X.M., Liu, C., Jiang, L.J., Li, Q.Y., Zhou, M.T., Cheng, T.C., Mita, K., Xia, Q.Y., 2015. A juvenile hormone transcription factor Bmdimm-fibroin H chain pathway is involved in the synthesis of silk protein in silkworm, *Bombyx mori*. J. Biol. Chem. 290, 972–986.

Zhao, X.M., Liu, C., Li, Q.Y., Hu, W.B., Zhou, M.T., Nie, H.Y., Zhang, Y.X., Peng, Z.C., Zhao, P., Xia, Q.Y., 2014. Basic helix-loop-helix transcription factor Bmsage is involved in regulation of fibroin H-chain gene via interaction with SGF1 in *Bombyx mori*. PLoS One 9, e94091.